# High-spin structures in 132Xe and 133Xe and evidence for isomers along the N=79 isotones

Vogt, A.; Siciliano, M.; Birkenbach, B.; Reiter, P.; Hadynska-Klek, K.; Wheldon, C.; Valiente-Dobón, J. J.; Teruya, E.; Yoshinaga, N.; Arnswald, K.; Bazzacco, D.; Blazhev, A.; Bracco, A.; Bruyneel, B.; Chakrawarthy, R. S.; Chapman, R.; Cline, D.; Corradi, L.; Crespi, F. C. L.; Cromaz, M.; de Angelis, G.; Eberth, J.; Fallon, P.; Farnea, E.; Fioretto, E.; Fransen, Ch.; Freeman, S. J.; Fu, B.; Gadea, A.; Gelletly, W.; Giaz, A.; Görgen, A.; Gottardo, A.; Hayes, A. B.; Hess, H.; Hetzenegger, R.; Hirsch, R.; Hua, H.; John, P. R.; Jolie, J; Jungclaus, A.; Karayonchev, V.; Kaya, L.; Korten, W.; Lee, I. Y.; Leoni, S.; Liang, X.; Lunardi, S.; Macchiavelli, A. O.; Menegazzo, R.

*Published in:*
Physical Review C

*DOI:*
10.1103/PhysRevC.96.024321

Published: 24/08/2017

*Document Version*
Publisher's PDF, also known as Version of record

# High-spin structures in $^{132}$Xe and $^{133}$Xe and evidence for isomers along the $N = 79$ isotones

A. Vogt,[1,*] M. Siciliano,[2,3] B. Birkenbach,[1] P. Reiter,[1] K. Hadyńska-Klęk,[3] C. Wheldon,[4] J. J. Valiente-Dobón,[3] E. Teruya,[5] N. Yoshinaga,[5] K. Arnswald,[1] D. Bazzacco,[6] A. Blazhev,[1] A. Bracco,[7] B. Bruyneel,[8] R. S. Chakrawarthy,[9] R. Chapman,[10] D. Cline,[11] L. Corradi,[3] F. C. L. Crespi,[7] M. Cromaz,[12] G. de Angelis,[3] J. Eberth,[1] P. Fallon,[12] E. Farnea,[6,†] E. Fioretto,[3] C. Fransen,[1] S. J. Freeman,[9] B. Fu,[1] A. Gadea,[13] W. Gelletly,[14] A. Giaz,[7] A. Görgen,[15,16,12] A. Gottardo,[3] A. B. Hayes,[11] H. Hess,[1] R. Hetzenegger,[1] R. Hirsch,[1] H. Hua,[11] P. R. John,[2,6] J. Jolie,[1] A. Jungclaus,[17] V. Karayonchev,[1] L. Kaya,[1] W. Korten,[16] I. Y. Lee,[12] S. Leoni,[7] X. Liang,[10] S. Lunardi,[2,6] A. O. Macchiavelli,[12] R. Menegazzo,[6] D. Mengoni,[18,2,6] C. Michelagnoli,[19] T. Mijatović,[20] G. Montagnoli,[2,6] D. Montanari,[21] C. Müller-Gatermann,[1] D. Napoli,[3] C. J. Pearson,[22] Zs. Podolyák,[14] G. Pollarolo,[23] A. Pullia,[7] M. Queiser,[1] F. Recchia,[2,6] P. H. Regan,[14,24] J.-M. Régis,[1] N. Saed-Samii,[1] E. Şahin,[15] F. Scarlassara,[2,6] M. Seidlitz,[1] B. Siebeck,[1] G. Sletten,[25] J. F. Smith,[10] P.-A. Söderström,[26] A. M. Stefanini,[3] O. Stezowski,[27] S. Szilner,[20] B. Szpak,[28] R. Teng,[11] C. Ur,[6] D. D. Warner,[29,†] K. Wolf,[1] C. Y. Wu,[30] and K. O. Zell[1]

[1]*Institut für Kernphysik, Universität zu Köln, D-50937 Köln, Germany*
[2]*Dipartimento di Fisica e Astronomia, Università di Padova, I-35131 Padova, Italy*
[3]*Istituto Nazionale di Fisica Nucleare, Laboratori Nazionali di Legnaro, I-35020 Legnaro, Italy*
[4]*School of Physics and Astronomy, University of Birmingham, Birmingham B15 2TT, United Kingdom*
[5]*Department of Physics, Saitama University, Saitama City 338-8570, Japan*
[6]*Istituto Nazionale di Fisica Nucleare, Sezione di Padova, I-35131 Padova, Italy*
[7]*Dipartimento di Fisica, Università di Milano and INFN Sezione di Milano, I-20133 Milano, Italy*
[8]*CEA Saclay, Service de Physique Nucleaire, F-91191 Gif-sur-Yvette, France*
[9]*Department of Physics and Astronomy, Schuster Laboratory, University of Manchester, Manchester M13 9PL, United Kingdom*
[10]*SUPA, School of Engineering and Computing, University of the West of Scotland, Paisley PA1 2BE, United Kingdom*
[11]*Department of Physics, University of Rochester, Rochester, New York 14627, USA*
[12]*Lawrence Berkeley National Laboratory, Berkeley, California 94720, USA*
[13]*Instituto de Física Corpuscular, CSIC - Universidad de Valencia, E-46071 Valencia, Spain*
[14]*Department of Physics, University of Surrey, Guildford, Surrey GU2 7XH, United Kingdom*
[15]*Department of Physics, University of Oslo, P.O. Box 1048 Blindern, N-0316 Oslo, Norway*
[16]*Institut de Recherche sur les lois Fondamentales de l'Univers - IRFU, CEA/DSM, Centre CEA de Saclay, F-91191 Gif-sur-Yvette Cedex, France*
[17]*Instituto de Estructura de la Materia, CSIC Madrid, E-28006 Madrid, Spain*
[18]*Nuclear Physics Research Group, University of the West of Scotland, High Street, Paisley PA1 2BE, Scotland, United Kingdom*
[19]*Institut Laue-Langevin (ILL), 38042 Grenoble Cedex 9, France*
[20]*Ruđer Bošković Institute, HR-10 002 Zagreb, Croatia*
[21]*USIAS - Universite de Strasbourg, IPHC-CNRS, F-67037 Strasbourg Cedex 2, France*
[22]*TRIUMF, 4004 Wesbrook Mall, Vancouver, British Columbia, V6T 2A3 Canada*
[23]*Dipartimento di Fisica Teorica dell'Università di Torino and INFN, I-10125 Torino, Italy*
[24]*Radioactivity Group, National Physical Laboratory, Teddington, Middlesex TW11 0LW, United Kingdom*
[25]*The Niels Bohr Institute, University of Copenhagen, Blegdamsvej 17, 2100 Copenhagen, Denmark*
[26]*RIKEN Nishina Center, Wako, 351-0198 Saitama, Japan*
[27]*Université de Lyon, Université Lyon-1, CNRS/IN2P3, UMR5822, IPNL, F-69622 Villeurbanne Cedex, France*
[28]*Henryk Niewodniczański Institute of Nuclear Physics PAN, PL-31342 Kraków, Poland*
[29]*CCLRC Daresbury Laboratory, Warrington WA4 4AD, United Kingdom*
[30]*Lawrence Livermore National Laboratory, Livermore, California 94551, USA*

(Received 9 June 2017; published 24 August 2017)

The transitional nuclei $^{132}$Xe and $^{133}$Xe are investigated after multinucleon-transfer (MNT) and fusion-evaporation reactions. Both nuclei are populated (i) in $^{136}$Xe + $^{208}$Pb MNT reactions employing the high-resolution Advanced GAmma Tracking Array (AGATA) coupled to the magnetic spectrometer PRISMA, (ii) in the $^{136}$Xe + $^{198}$Pt MNT reaction employing the GAMMASPHERE spectrometer in combination with the gas-detector array CHICO, and (iii) as an evaporation residue after a $^{130}$Te$(\alpha,xn)^{134-xn}$Xe fusion-evaporation reaction employing the HORUS $\gamma$-ray array at the University of Cologne. The high-spin level schemes are considerably extended above the $J^\pi = (7^-)$ and $(10^+)$ isomers in $^{132}$Xe and above the $11/2^-$ isomer in $^{133}$Xe. The results are compared to the high-spin systematics of the $Z = 54$ as well as the $N = 78$ and $N = 79$ chains. Furthermore, evidence is found for a long-lived ($T_{1/2} \gg 1\ \mu$s) isomer in $^{133}$Xe which closes a gap along the $N = 79$

*Corresponding author: andreas.vogt@ikp.uni-koeln.de
†Deceased.

 

isotones. Shell-model calculations employing the SN100PN and PQM130 effective interactions reproduce the experimental findings and provide guidance to the interpretation of the observed high-spin features.

DOI: 10.1103/PhysRevC.96.024321

## I. INTRODUCTION

The $50 \leqslant N, Z \leqslant 82$ region of the Segrè chart, spanning the nuclei "northwest" of doubly-magic $^{132}$Sn, is an intriguing study ground to test the suitability and predictive power of nuclear models at both low and high spins. Low-spin excited states in the nearly spherical nuclei near proton- and neutron-shell closures are well described as anharmonic vibrations [1] with a gradual change to rotational structures further away from the closed shells. Further on, quasiparticle excitations play a key role and are responsible for the presence of yrast-trap isomers. These long-lived states interrupt and fragment the decay flux in spectroscopic investigations. High-$j$ couplings involving the unique-parity $h_{11/2}$ neutron-hole orbital give rise to a wealth of high-spin states with multi-quasiparticle character. In particular, detailed knowledge of isomers is crucial to ascertain the active quasiparticle configurations in the specific nucleus.

$^{132}$Xe and $^{133}$Xe are located in the proton midshell between the $Z = 50$ shell and the $Z = 64$ subshell closures. Three and four neutrons away from the $N = 82$ shell closure, the respective Xe isotopes have come within reach of advanced untruncated shell-model calculations. Several recently developed effective shell-model interactions [2–7] take aim toward a unified description of the $50 \leqslant N, Z \leqslant 82$ region.

The available data on low-spin states in both $^{132}$Xe and $^{133}$Xe originate from earlier work employing $\beta$ decay, Coulomb excitation [8–10], and neutron scattering [11]. Intermediate-spin states were investigated via $^{130}$Te$(\alpha,2n\gamma)$ [12] and $^{130}$Te$(\alpha,n\gamma)$ [13] reactions, respectively. The lack of suitable stable beam-target combinations obstructs the population of high-spin states via fusion-evaporation processes involving higher-mass reaction partners. Multinucleon-transfer (MNT) reactions offer an efficient gateway to moderately neutron-rich nuclei that cannot be reached by means of fusion-evaporation reactions. These heavy-ion collisions proved to be capable of populating both high spins and excitation energies. The identification of the often elusive multinucleon-transfer channels takes advantage of the high analyzing power of modern detector arrays and mass spectrometers [14,15].

Isomeric $J^\pi = 10^+$ states were reported in all even-mass $N = 78$ isotones from $^{128}$Sn up to $^{142}$Gd. The states are interpreted as fully aligned $\nu h_{11/2}^{-2}$ two-neutron hole configurations. A decreasing trend in lifetimes is observed with increasing proton number $Z$ [12,16–22]. Compared to the other $N = 78$ isotones, the yrast $10_1^+$ state in $^{132}$Xe has an exceptionally long half-life of $T_{1/2} = 8.39(11)$ ms [23] and decays predominantly via an 538-keV $E3$ $\gamma$ ray to the $(7_1^-)$ state, whereas the location of the $8_1^+$ state in the level scheme is still unknown [8]. In fact, the long half-life suggests that the $10_1^+$ state might be located very close to the $8_1^+$ state. The $(7_1^-)$ state in $^{132}$Xe is also an isomer with a half-life of $T_{1/2} = 87(3)$ ns and a $\nu(h_{11/2}^{-1} d_{3/2}^{-1})$ configuration [12,24].

For the odd-mass $50 \leqslant N, Z \leqslant 82$ nuclei, a long-lived $11/2^-$ isomer above the $3/2^+$ ground state is a typical feature which is also present in $^{133}$Xe at 233.221(15) keV with a half-life of 2.198(13) days [9]. Lönnroth *et al.* [13] assigned three $\gamma$ rays with energies of 247.4, 947.8, and 695.2 keV to form a $(23/2^-) \rightarrow 19/2_1^- \rightarrow 15/2_1^- \rightarrow 11/2_1^-$ cascade on top of the $11/2^-$ isomer. Firm spin-parity assignments in the intermediate-spin regime were made up to $J^\pi = 19/2^-$. Along the $N = 79$ chain [partial level schemes presented in Figs. 1(a) to 1(f)], $J^\pi = (23/2^+)$ isomers were reported in $^{129}$Sn [$T_{1/2} = 2.22(14)$ $\mu$s at 1762 keV] [25,26], $^{131}$Te [93(12) ms at 1941 keV] [27], and $^{139}$Nd [277(2) ns at 2617 keV] [28]. These states are explained as $\nu(h_{11/2}^{-2} d_{3/2}^{-1})$ configurations [26,29,30]. Further $J^\pi = 19/2^+$ isomers below and $J^\pi = 27/2^-$ isomers above the $23/2^+$ state were observed with half-lives in the ns to $\mu$s regime in $^{129}$Sn [31,32].

First spectroscopic data on the $(23/2^+)$ isomer in $^{131}$Te were obtained in a $^{64}$Ni + $^{130}$Te multinucleon-transfer experiment at the GASP $\gamma$-ray spectrometer [33]. A 361-564-833-keV triple coincidence was assigned to a $(21/2^-) \rightarrow (19/2^-) \rightarrow (15/2^-) \rightarrow 11/2^-$ band based on isotopic systematics. A delayed component ($T_{1/2} \gg 1$ $\mu$s) in the off-beam spectra led to the assumption that a $23/2^+$ isomer was located above the $(21/2^-)$ state. Fogelberg *et al.* determined a very long half-life of 93(12) ms employing thermal fission of U isotopes at the OSIRIS mass separator [34] and assigned an $E3$ character to the 361-keV transition. Furthermore, a conversion-electron measurement corroborated that only the 361-keV transition is the delayed transition depopulating the $(23/2^+)$ state. Finally, the $15/2_1^-$ and $19/2_1^-$ levels were confirmed and a prompt negative-parity cascade was added to the level scheme by Astier *et al.* [29]. The half-life of the $(23/2^+)$ state was constrained to be longer than 10 $\mu$s and the decay to the $19/2_1^-$ state was reaffirmed to be of $M2$ character. Based on the OSIRIS result, a reduced transition strength of $B(M2; 23/2_1^+ \rightarrow 19/2_1^-) = 2 \times 10^{-6}$ W.u. was deduced [29].

The elusive $23/2^+$ isomer in $^{139}$Nd was first reported by Müller-Veggian *et al.* who observed a long-living delayed component in off-beam $\gamma\gamma$-coincidence spectra and reported a first lower half-life limit [35]. Later, the isomer's location was constrained to be above the $19/2_1^+$ state and a first precise half-life of $T_{1/2} = 272(4)$ ns could be obtained [36]. Recently, in 2013, Vancraeyenest *et al.* [30] confirmed these results employing the sophisticated Jyväskylä recoil-decay tagging setup. The group finally achieved an unambiguous placement of the isomer in the level scheme as it is populated by the decay of three higher-lying $(25/2^-)$ states. In $^{137}$Ce, a $J = (31/2)$ state was observed to be isomeric with a half-life of 5 ns [37]. Up to now, no high-lying isomeric states have been reported for $^{133}$Xe and $^{135}$Ba. Any experimental information on high-spin states is missing for $^{132}$Xe beyond 2.8 MeV and for $^{133}$Xe beyond 2.1 MeV. The scarce experimental data together with

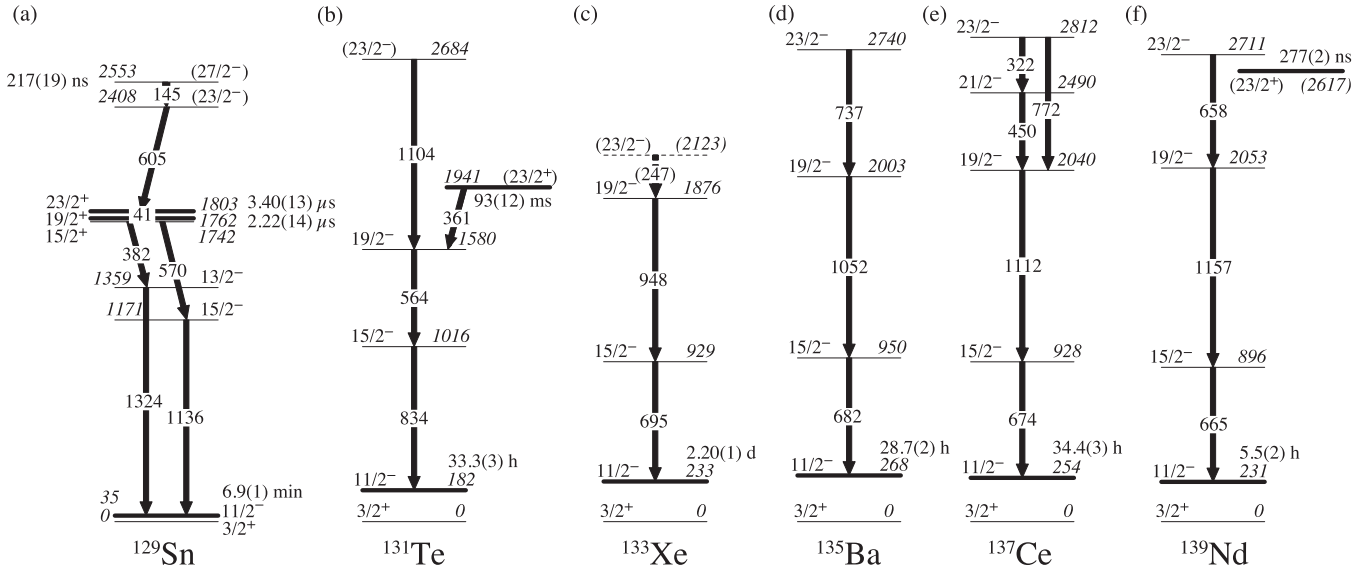


FIG. 1. Comparison of high-spin states and isomer half-lives along the $N = 79$ isotones ranging from $^{129}$Sn to $^{139}$Nd; data are taken from Refs. [13,25,28–30,32,38–40]. Tentative assignments are written in parentheses. See text for details.

recent theoretical advances motivate a refined investigation of high-spin features in both nuclei.

In this article, we report and discuss new results for the high-spin regimes of $^{132}$Xe and $^{133}$Xe. Excited states of $^{132}$Xe and $^{133}$Xe were populated in three different experiments: The combination of the high-resolution position-sensitive Advanced GAmma Tracking Array (AGATA) [41] and the PRISMA magnetic mass spectrometer [42–44] was employed to study the nuclei after $^{136}$Xe + $^{208}$Pb multinucleon transfer. Moreover, excited states in both nuclei were populated after a $^{136}$Xe + $^{198}$Pt MNT reaction employing the GAMMASPHERE+CHICO setup [45,46] at Lawrence Berkeley National Laboratory (LBNL). The $^{130}$Te$(\alpha,n)^{133}$Xe and $^{130}$Te$(\alpha,2n)^{132}$Xe fusion-evaporation reactions were utilized in a third experiment employing the High-efficiency Observatory for $\gamma$-Ray Unique Spectroscopy (HORUS) [47] at the Institute of Nuclear Physics, University of Cologne.

During the preparation of this manuscript, we became aware of a parallel study of $^{133}$Xe by Reed, Lane *et al.* [48]. The results are consistent with those presented in the current work.

This paper is organized as follows: the experimental setup and data analysis of the three experiments are described in Sec. II, followed by the experimental results in Sec. III. A comparison with modern shell-model calculations is presented in Sec. IV before the paper closes with a summary and conclusions.

## II. EXPERIMENTAL PROCEDURE AND DATA ANALYSIS

$^{132}$Xe and $^{133}$Xe were populated in a $^{136}$Xe + $^{208}$Pb multinucleon-transfer experiment at the Laboratori Nazionali di Legnaro, Italy. In this experiment, a 6.84 MeV/nucleon $^{136}$Xe beam was accelerated by the PIAVE+ALPI accelerator complex onto a 1-mg/cm$^2$ $^{208}$Pb target. The Advanced GAmma Tracking Array (AGATA) [41] in a first demonstrator configuration [49] was placed at a distance of 18.8 cm from the target position to measure $\gamma$ rays from excited states. The array consisted of nine large-volume electronically segmented high-purity Ge (HPGe) detectors in three triple cryostats [50]. An isotopic identification of the nuclei of interest was provided by the magnetic spectrometer PRISMA placed at the reaction's grazing angle of $\theta_{\text{lab}} = 42^\circ$. An event registered by the PRISMA focal-plane detector in coincidence with an AGATA event was taken as a trigger for the data acquisition. Pulse-shape analysis of the digitized detector signals was applied to determine the individual interaction points within the HPGe shell [51], enabling the Orsay forward-tracking algorithm [52] to reconstruct the individual emitted $\gamma$-ray energies and to determine the first interaction point of the $\gamma$ ray in the germanium and, thus, the emission angle. Together with the kinematic information from PRISMA, a precise Doppler correction is performed. Furthermore, the fully reconstructed momentum vector of the ejectile nucleus enables a reconstruction of the total kinetic energy loss (TKEL) of the reaction by assuming a binary process and by incorporating the excitation energies of both binary partners. The TKEL is defined as the reaction's $Q$-value distribution with an opposite sign [43,53].

In a second experiment, the 88-Inch Cyclotron facility at LBNL provided a 6.25-MeV/nucleon $^{136}$Xe beam that impinged onto a 92% isotopically enriched self-supporting 420-$\mu$g/cm$^2$ $^{198}$Pt target. The GAMMASPHERE array, which in this experiment consisted of 103 Compton-suppressed HPGe detectors, was employed for $\gamma$-ray spectroscopy [45]. Both polar and azimuthal angles and the time-of-flight difference $\Delta t_{\text{TOF}}$ between the detection of beam-like and target-like reaction products were measured with the gas-filled parallel plate avalanche chamber ancillary detector CHICO, allowing for an event-by-event Doppler-shift correction for emitted $\gamma$ rays. The time window for prompt events was set to $\pm$45 ns around the master trigger, requiring three prompt $\gamma$ rays and the binary fragments being detected in CHICO; the one

for the delayed $\gamma$ rays was set from 45 to 780 ns. Further details are given in Ref. [24]. The data of the experiment were sorted into four two-dimensional matrices gated on beam-like fragments: (i) an in-beam Doppler-corrected prompt $\gamma\gamma$ matrix, (ii) an out-of-beam delayed-delayed $\gamma\gamma$ matrix, (iii) a delayed-prompt $\gamma\gamma$ matrix, and (iv) a delayed $\gamma$-time matrix. The RADWARE analysis software [54] was used to project and background-subtract the gated spectra.

Furthermore, $^{132}$Xe and $^{133}$Xe were populated via the fusion-evaporation reaction $^{130}$Te$(\alpha,xn)^{134-xn}$Xe, employing a 19-MeV $\alpha$ beam delivered by the FN Tandem accelerator located at the Institute for Nuclear Physics, University of Cologne. The $^{130}$Te target with a thickness of 1.8 mg/cm$^2$ was evaporated onto a 120 mg/cm$^2$ thick Bi backing plus a 132 mg/cm$^2$ thick Cu layer for heat dissipation. All residual reaction products as well as the beam were stopped inside the Bi backing. $\gamma$ rays from excited states were measured employing the Cologne fast-timing setup, comprising eight HPGe detectors from the HORUS array [47] and eight $LaBr_3$:Ce scintillators. The count rate of the individual HPGe crystals was maintained around 20 kHz during the experiment. Coincident events were processed and recorded utilizing the synchronized 80-MHz XIA Digital Gamma Finder (DGF) data-acquisition system and stored to disk. The data were analyzed offline using the SOCO-V2 [55,56] and TV [57] codes. Recorded $\gamma$ rays were sorted into (i) a general symmetrized two-dimensional matrix to study $\gamma\gamma$ coincidence relations, (ii) a three-dimensional cube, and (iii) a total of six group matrices each corresponding to different relative angles $\theta_1$, $\theta_2$, and $\phi$ between all HPGe detector pairs with respect to the beam axis to investigate multipolarities via angular correlations.

Spins and parities of excited states are investigated with the $\gamma\gamma$ angular-correlation code CORLEONE [59,60] employing the DCO (directional correlation from oriented states) formalism based on the phase convention by Krane, Steffen, and Wheeler [61,62]. The angular distribution of two coincident $\gamma$ rays in a recoiling nucleus, subsequently emitted from the initial state $J_1$ through an intermediate state $J_2$ to the final state $J_3$, is described by the following equation:

$$W(\theta_1,\theta_2,\phi) = \sum_{\lambda,\lambda_1,\lambda_2} B_{\lambda_1}(J_1) A_\lambda^{\lambda_1\lambda_2}(\gamma_1,\delta_1) A_{\lambda_2}(\gamma_2,\delta_2) \times H_{\lambda\lambda_1\lambda_2}(\theta_1,\theta_2,\phi), \quad (1)$$

where $B_{\lambda_1}(J_1)$ is a statistical tensor describing the orientation of the initial state with respect to the orientation axis. Correlation coefficients $A_\lambda^{\lambda_1\lambda_2}$ and $A_{\lambda_2}$ parametrize the spins $J_i$ and multipole-mixing ratios $\delta_i$ of the corresponding transitions between the excited states of interest. The angular-correlation function $H_{\lambda\lambda_1\lambda_2}(\theta_1,\theta_2,\phi)$ depends on the polar angles of emission $\theta_1$ and $\theta_2$ of $\gamma_1$ and $\gamma_2$ in the polarization plane and on the azimuthal rotation $\phi$ of the emission (cf. Fig. 2 for further definition). The tensor ranks $\lambda_1$ and $\lambda_2$ describe the orientation of the states $J_1$ and $J_2$, and $\lambda$ is defined as the tensor rank of the radiation field. Detailed expressions for the coefficients $A_\lambda^{\lambda_1\lambda_2}$, $A_{\lambda_2}$, $B_{\lambda_1}$, and $H_{\lambda\lambda_1\lambda_2}$ are given in Ref. [62]. Different hypotheses of involved spins and multipole-mixing ratios are evaluated in $\chi^2$ fits of experimental transition intensities in the different angular-correlation groups to the correlation function

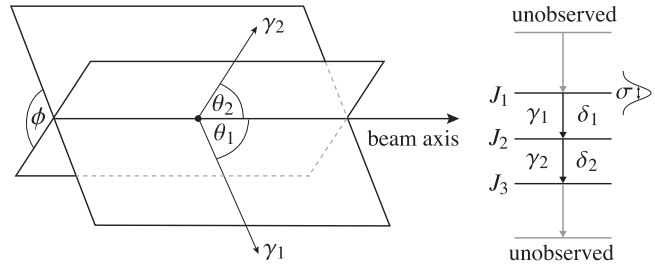


FIG. 2. Correlation of two coincident $\gamma$ rays between excited states of spin $J_i$. The transitions are further characterized by their multipole-mixing ratios $\delta_i$ (adapted from Ref. [58]).

$W(\theta_1,\theta_2,\phi) \equiv W(J_1,J_2,J_3,\delta_1,\delta_2,\sigma)$. The parameter $\sigma$ denotes the width of the alignment distribution, i.e., the distribution of the magnetic substates $m$ of $J_1$.

A small anisotropic behavior of theoretically isotropic $\gamma$-ray transitions required a correction of the measured intensities in the individual angular-correlation groups [63]. This anisotropy of the efficiency-corrected intensities is mainly caused by different dead times in the digital data-acquisition system as count rates differed between the $^{226}$Ra efficiency-calibration source run and the actual experiment. A fit to the well-known $4_1^+ \rightarrow 2_1^+ \rightarrow 0_1^+$ cascade in $^{132}$Xe, comprising two pure electric quadrupole transitions, was used to renormalize the initial efficiency-corrected intensities of the angular-correlation groups to their theoretical values with the assumption that both transitions are of pure $E2$ character. The anisotropy corrections are in the order of 2% to 11% and were subsequently applied to fits of other cascades.

## III. RESULTS

### A. $^{132}$Xe

A partial level scheme of $^{132}$Xe obtained in the present work is displayed in Fig. 3 (followed by the level scheme for $^{133}$Xe in Fig. 4). Intensities above the isomers are extracted from the in-beam $^{136}$Xe + $^{208}$Pb data and normalized to the intensity of the 650-keV transition. Correlations of the reconstructed TKEL with coincident prompt in-beam $\gamma$ rays of AGATA allow the total excitation energy of the nucleus of interest to be restricted. Gates on different TKEL regions either suppress or enhance $\gamma$-ray transitions between states with different excitation energies and angular momenta. Due to the presence of the two long-lived isomers in the level scheme of $^{132}$Xe, TKEL gates allow for a discrimination between $\gamma$-ray transitions below and above the isomeric states. AGATA $\gamma$-ray spectra of $^{132}$Xe identified in PRISMA are presented in Fig. 5 with gates on (a) small TKEL and (b) large TKEL. The applied gates are shown in the corresponding insets. The 668-keV $2_1^+ \rightarrow 0_1^+$, 727-keV $5_1^+ \rightarrow 4_1^+$, and 773-keV $4_1^+ \rightarrow 2_1^+$ transitions dominate the low-TKEL gated $\gamma$-ray spectrum, which can be attributed to the low-spin structure below the isomers [8]. In contrast, all transitions between low-spin states are completely suppressed with the gate on large TKEL. Seven new $\gamma$-ray transitions with energies of 208, 298, 476, 559, 650, 1133, and 1240 keV are observed in this spectrum. A new 940-keV line is visible in Fig. 5(a).

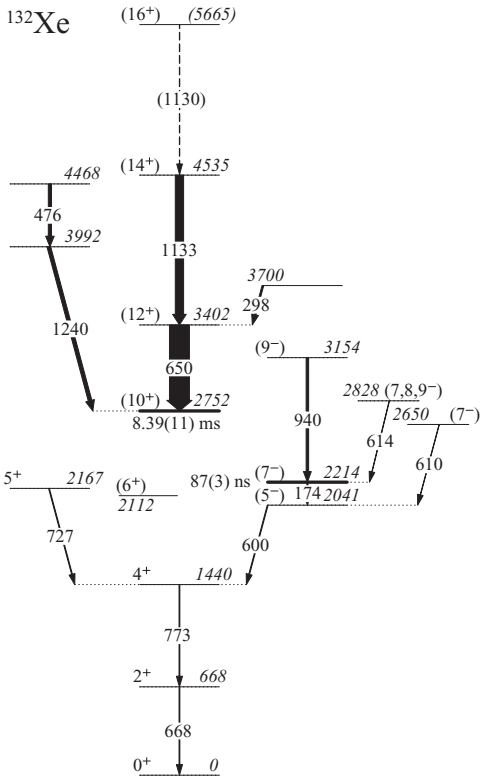


FIG. 3. Partial level scheme of $^{132}$Xe with the newly observed $\gamma$ rays above the 8.39(11)-ms $(10^+_1)$ and 87-ns $(7^-_1)$ isomers. Energies are given in keV. Intensities above the isomers are extracted from the in-beam $^{136}$Xe + $^{208}$Pb AGATA data and normalized to the intensity of the 650-keV transition.

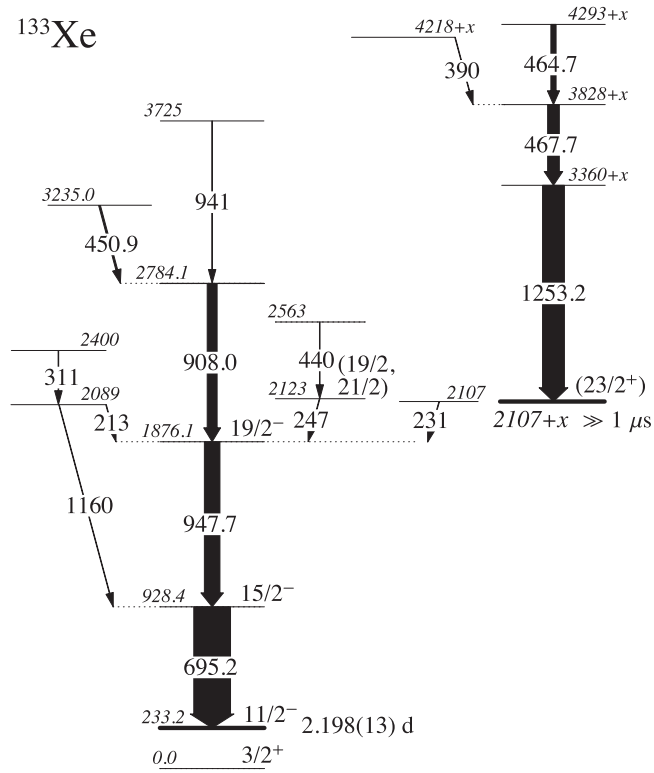


FIG. 4. Partial level scheme of $^{133}$Xe. Energies are given in keV. Intensities above the isomers are extracted from the in-beam $^{136}$Xe + $^{208}$Pb AGATA data and normalized to the intensity of the 695-keV transition.

$\gamma\gamma$ coincidences are exploited in the $^{136}$Xe + $^{198}$Pt dataset. The 650- and 1133-keV, as well as the 1240- and 476-keV transitions are mutually coincident. Corresponding gated spectra are depicted in Figs. 5(e) to 5(h). Correlations of prompt transitions populating isomers with the respective depopulating $\gamma$ rays were enabled by the $^{136}$Xe + $^{198}$Pt experiment. Delayed-prompt $\gamma\gamma$ coincidences with a gate on the delayed 668-keV $2^+_1 \rightarrow 0^+_1$ transition are presented in Fig. 5(h). The 8.39(11)-ms half-life of the $(10^+)$ isomer is too long to observe delayed-prompt coincidences within the experimental time window. Instead, a gate on the delayed transitions provides a spectrum only containing the transitions feeding the 87(3)-ns $7^-$ isomer. The corresponding half-life of the delayed component of the 668-keV transition used in the gate is validated to be 88(5) ns. Consequently, the 940-keV transition is placed on top of the 2214-keV state. The line at 614 keV is identified as the decay of a $(7,8,9^-)$ state, previously observed in a $\beta$-decay study of $^{132m}$I [64]. Other lines visible in Fig. 5(h) at 348, 373, 402, 451, 783, and 869 keV are not observed in the AGATA spectra. Since the high-lying 650-, 1133-, 476-, and 1240-keV $\gamma$-ray transitions are not present in the delayed-prompt coincidence spectrum, these transitions have to feed the $(10^+)$ isomer. The intensity balance suggests the 1133-keV transition to be placed above the 650-keV $\gamma$ ray feeding the $(10^+)$ isomer. Furthermore, the 1133-keV transition is in coincidence with another close-lying line at 1130 keV. A peak at 1130 keV is also visible in the AGATA data; thus, the transition is tentatively placed on top of the 4535-keV state. With no connection to the 1133-650-keV cascade, the 1240- and 476-keV $\gamma$-ray cascade is tentatively placed parallel, assuming no unobserved low-energy $\gamma$ ray. A 298-keV transition feeds the new 3402-keV state. Excited states above the $(10^+)$ level were not measured in the HORUS experiment.

### B. $^{133}$Xe

The level scheme of $^{133}$Xe obtained in the present work is presented in Fig. 4. Again, intensities are extracted from the in-beam $^{136}$Xe + $^{208}$Pb data and normalized to the intensity of the 695-keV transition. AGATA $\gamma$-ray spectra of $^{133}$Xe identified in PRISMA are presented in Fig. 6 with gates on (a) small TKEL and (b) large TKEL. The applied gates are shown in the corresponding insets (c) and (d). The small-TKEL gated spectrum exhibits several transitions between known positive-parity states with small excitation energies. Peaks located at 695.2 and 947.6 keV are identified as members of the previously known negative-parity band on top of the long-lived $11/2^-_1$ state. The intensities of these $15/2^-_1 \rightarrow 11/2^-_1$ and $19/2^-_1 \rightarrow 15/2^-_1$ transitions are significantly enhanced in the spectrum gated on large TKEL. Further previously unknown peaks at 450.9, 464.7, 467.7, 654, 908.0, 941, 1096, 1160, and 1253.2 keV are observed in Fig. 6(b). An analysis of the prompt $\gamma\gamma$ matrix obtained with GAMMASPHERE yields

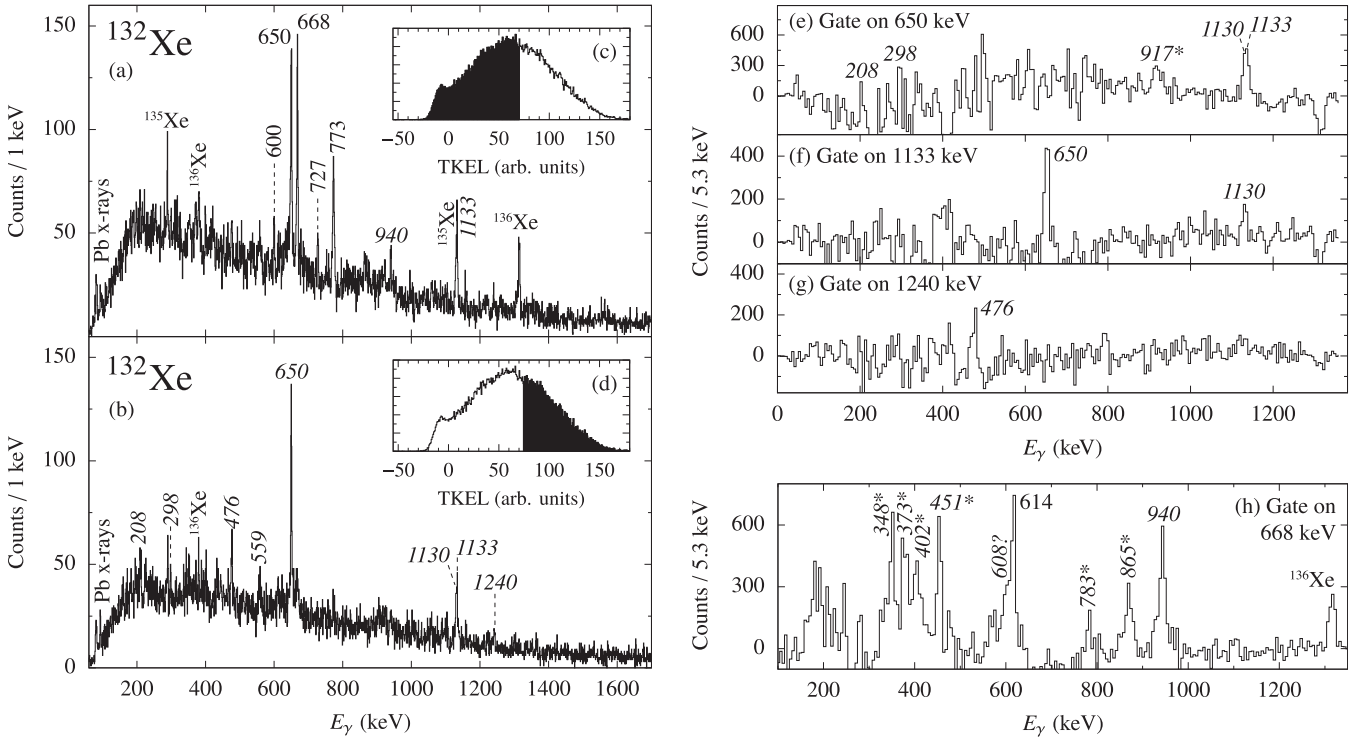


FIG. 5. Left: AGATA $\gamma$-ray spectra for $^{132}$Xe identified with PRISMA after the $^{136}$Xe + $^{208}$Pb MNT reaction. (a) Gate on small TKEL. (b) Gate on large TKEL; the transitions below the long-lived $(10^+_1)$ and $(7^-_1)$ isomers are not present any more. The applied gates on the TKEL distributions are presented in the insets (c) and (d). Previously unknown $\gamma$ rays are labeled with italic characters. Right, (e)–(g): Prompt GAMMASPHERE $\gamma\gamma$ coincidences from the $^{136}$Xe + $^{198}$Pt experiment, gated on 650, 1133, and 1240 keV. (h) Delayed-prompt GAMMASPHERE coincidence spectrum with a gate on the delayed 668-keV $2^+_1 \rightarrow 0^+_1$ transition. Asterisks mark transitions not observed in the HORUS and AGATA experiments. See text for details.

coincidences between the 695.2- and 947.7-keV $\gamma$ rays and the newly observed 450.9- and 908.0-keV transitions [cf. Fig. 6(e)]. The 908.0-keV transition has to be placed on top of the 1876.1-keV state, which is further supported by the HORUS $\gamma\gamma$ coincidences. As presented in Figs. 6(h) and 6(j), both gates on 695 and 948 keV show coincident 908-keV peaks. Vice versa, a gate on 908 keV, although contaminated by the 910.1-keV decay of the 2350.6-keV level in $^{132}$Xe [8], shows clear mutual coincidence with the two established $\gamma$-ray transitions. Also the 695-, 1160- and 311-keV $\gamma$-ray transitions are coincident with each other in $\gamma\gamma$ gates [cf. Figs. 6(h) and 6(k)]. The newly established state at 2089 keV decays via a 213-keV $\gamma$-ray to the $19/2^-_1$ state. The 213-keV transition also appears in the prompt GAMMASPHERE data in gates on 695 and 948 keV.

As observed in the prompt GAMMASPHERE $\gamma\gamma$ coincidences in Figs. 6(f) and 6(g), the 1253-keV $\gamma$-ray transition is mutually coincident to the ones at 465 and 468 keV. Moreover, these three $\gamma$ rays appear only for gates on large TKEL in Fig. 6(b). Thus, the transitions have to be located at comparatively large excitation energies. However, there is no connection to any previously observed $\gamma$ ray: neither to the bands based on the previously known positive-parity states nor to the negative-parity states above the $11/2^-_1$ state. This observation corroborates the presence of a yet unobserved isomer in $^{133}$Xe, fed by the 464.7-, 467.7-, and 1253.2-keV $\gamma$ rays. A 390-keV transition is coincident to 468 and 1253 keV and placed parallel to the 465-keV transition. Based on intensity relations and $\gamma\gamma$ coincidences, the 451- and 941-keV transitions are placed parallel, feeding the 2784-keV state. The 654- and 1096-keV $\gamma$-ray transitions are not visible in the coincidence data. None of the known transitions between low-spin or negative-parity intermediate-spin states appear in the delayed GAMMASPHERE data. Consequently, in accordance with previous studies performed with the GAMMASPHERE dataset [24], the half-life of the new isomer is estimated to be $T_{1/2} \gg 1\ \mu$s.

Strong peaks at 231- and 247-keV are mutually coincident with 695- and 948-keV lines in the HORUS dataset. The 231-keV transition is not to be confused with the isomeric 233.2-keV transition from the $11/2^-_1$ state to the ground state, which is too weak to be observed. No coincidence is found with the 908-keV $\gamma$ ray. Moreover, triple-$\gamma$ coincidences and intensity relations support the placement of a 440-keV $\gamma$ ray on top of the 247-keV transition. Although these transitions are clearly visible in the HORUS coincidence data, neither of them are observed in the AGATA or in the GAMMASPHERE in-beam data. Arrows mark the expected positions in Figs. 6(a) and 6(b). The 247-keV $\gamma$ ray was first reported by Lönnroth *et al.* [13]. The group measured an $\ell = 2$ multipolarity and assigned a $(23/2^-) \rightarrow 19/2^-_1$ transition. An $M2$ character was excluded since no delayed component was observed in the data. Due to

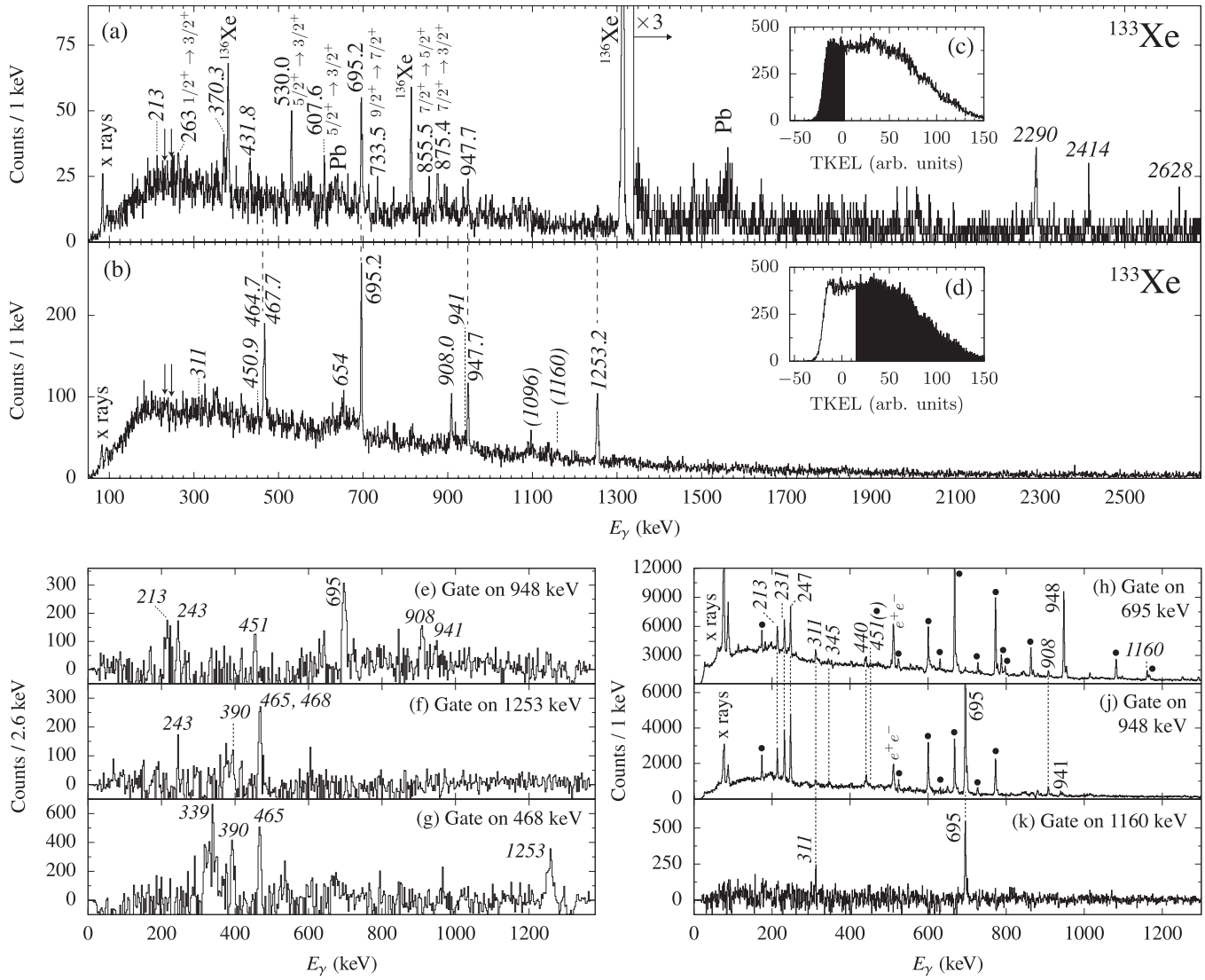


FIG. 6. AGATA $\gamma$-ray spectra of $^{133}$Xe selected by PRISMA with gates on (a) small TKEL and (b) large TKEL; corresponding TKEL spectra in (c) and (d) with gates marked in black. Previously unknown $\gamma$-ray transitions are labeled with italic characters. Arrows label the supposed positions of the 231- and 247-keV $\gamma$-ray transitions. (e)–(g) GAMMASPHERE prompt $\gamma\gamma$ coincidences with gates on 948, 1253, and 468 keV. (h), (j), (k) HORUS prompt $\gamma\gamma$ coincidences with gates on 695, 948, and 1160 keV. Contaminations originating from the dominating $2n$ evaporation channel $^{132}$Xe are labeled with filled black circles.

the prompt character of the 213- and 908-keV transitions in both AGATA and GAMMASPHERE experiments, both the 2089- and 2784-keV states can be excluded to be isomeric or as a corresponding decay path of an isomeric state.

Spin assignments can be tested in the HORUS experiment with the procedure discussed in Sec. II. Angular-distribution functions $W(\theta_1,\theta_2,\phi)$ of two coincident $\gamma$-ray transitions are fitted to experimental $\gamma$-ray intensity distributions obtained by gates on depopulating transitions in the $\gamma\gamma$-coincidence matrices of six angular-correlation groups. Figure 7(a) shows a benchmark angular-correlation fit of the 727-keV $5_1^+ \rightarrow 4_1^+$ decay from the quasi-$\gamma$ band of $^{132}$Xe. Anisotropy corrections to the intensity distributions, applied to all six angular-correlation groups, are validated in this way. The fit of a $5^+ \xrightarrow{\delta} 4^+ \xrightarrow{E2} 2^+$ hypothesis yields a good agreement with the experimental distribution. Moreover, the obtained $E2/M1$ multipole-mixing ratio of $\delta_{\text{exp.}} = +0.40(5)$ compares well with the evaluated value of $\delta_{\text{lit.}} = +0.41^{+7}_{-8}$ [8]. Similarly, Fig. 7(b) shows angular correlations for the 247-948-keV cascade in $^{133}$Xe. Obviously, a pure $E2$ transition does not fit the data. A $19/2 \xrightarrow{\delta} 19/2^- \rightarrow 15/2^-$ hypothesis with $\delta = -0.69(11)$ ($\chi^2 = 0.8$) yields the best agreement with the experimental $W(\theta_1,\theta_2,\phi)$ distribution. Nevertheless, based on the fit quality, neither a $21/2 \xrightarrow{\delta} 19/2^-$ scenario with $\delta = +0.24(3)$ (slightly worse agreement with $\chi^2 = 3.7$) nor a $23/2 \xrightarrow{\delta} 19/2^-$ transition with $\delta = -0.32(6)$ ($\chi^2 = 5.4$) can be entirely excluded. Statistics are not sufficient to perform fits for the 213-, 231-, and 1160-keV $\gamma$-ray transitions.

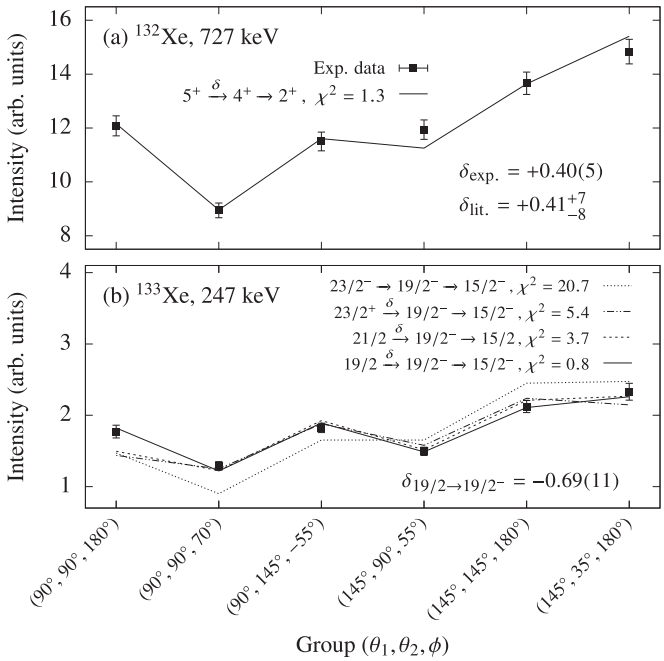


FIG. 7. (a) $\gamma\gamma$ angular correlations for the $5_1^+ \xrightarrow{\delta} 4_1^+ \xrightarrow{E2} 2_1^+$ 727-773-keV cascade in $^{132}$Xe. Experimental values (data points) are compared to calculated angular-correlation functions $W(\theta_1,\theta_2,\phi)$ (lines) for six correlation groups $(\theta_1,\theta_2,\phi)$ using the code CORLEONE. The known multipole-mixing ratio of the 727-keV transition in $^{132}$Xe is well reproduced by the CORLEONE calculation. (b) Same as (a), but for the 247-948-keV cascade in $^{133}$Xe. Several spin hypotheses are plotted. The $19/2 \xrightarrow{\delta} 19/2^- \rightarrow 15/2^-$ hypothesis (solid line) with $\delta = -0.69(11)$ yields the best agreement.

## IV. DISCUSSION

Shell-model calculations for both positive- and negative-parity states were performed in the $50 \leqslant Z,N \leqslant 82$ single-particle space generated by the valence nucleons occupying the $0g_{7/2}$, $1d_{5/2}$, $1d_{3/2}$, $2s_{1/2}$, and $0h_{11/2}$ orbitals. Two different interactions were employed: (i) The first calculation was carried out using a phenomenological interaction, called PQM130 (Pairing + Quadrupole-Quadrupole + Multipole for mass region 130), constructed from a pairing-plus-quadrupole interaction that consists of spherical single-particle energies, a monopole-pairing interaction, a quadrupole-pairing interaction, and a quadrupole-quadrupole interaction. It is combined with newly introduced higher multipole-pairing interactions. Valence neutrons and protons are treated as holes and particles relative to the closed shells. Details on the calculation are given in Ref. [4]. (ii) The second calculation was performed in the above mentioned model space (also called jj55pn) outside $^{100}$Sn using the jj55pna Hamiltonian [2] (referred to as the SN100PN interaction) employing the computer code NUSHELLX@MSU [65] without any truncations. The SN100PN interaction is constructed from a renormalized $G$ matrix derived from the CD-Bonn nucleon-nucleon interaction [66]; single-particle energies are deduced from the experimentally observed level energies in $^{133}$Sb and $^{131}$Sn. The interaction has four parts: neutron-neutron, neutron-proton, proton-proton, and Coulomb repulsion between the protons.

A comparison of experimental energy spectra with the results of the shell-model calculations is presented in Fig. 8 for (a) $^{132}$Xe and (b) $^{133}$Xe. Both calculations reproduce the hitherto known members of the yrast ground-state band of $^{132}$Xe quite well. Furthermore, both interactions reproduce the position of the $5_1^+$ state. However, the $3_1^+$ and $4_2^+$ states are interchanged in the SN100PN calculation, while in the PQM130 calculation the $4_2^+$ state is calculated to be above the $6_1^+$. The negative-parity $5_1^-$, $7_1^-$, and $7_2^-$ states are well reproduced by the SN100PN interaction; on the other hand, $5_1^-$ and $7_1^-$ states are permuted in the PQM130 calculation. Another ambiguity remains for the ordering of the $7_2^-$ and $8_1^-$ states. The experimental location of the $8_1^+$ state is still experimentally unresolved. The SN100PN calculation predicts the state to be degenerate with the $10_1^+$ state in excitation energy, whereas the PQM130 interaction computes the first two $8^+$ levels below the $10_1^+$ state. Earlier pair-truncated shell-model calculations predicted the yrast $8_1^+$ about 0.05 MeV above the $10_1^+$ state [67]. The next even-even isotope $^{134}$Xe exhibits a $10_1^+ \rightarrow 8_1^+$ transition of 28 keV. Likewise, in $^{130}$Te the corresponding transition amounts to only 18 keV [17]. Backbending phenomena in the yrast bands were observed systematically in $^{122-130}$Xe, among others, visible in a reduced energy spacing between the $8_1^+$ and $10_1^+$ states [68]. It is explained by the band crossing of the quasi-ground-state band with another quasiband with a $\nu(h_{11/2}^2)$ configuration [68]. As mentioned in Sec. I, the long 8.39(11)-ms half-life of the $10_1^+$ state and its dominant $E3$ decay to the $7_1^-$ state even suggest a placement below the $8_1^+$ state. Therefore, each assignment above the $10_1^+$ state is tentative. Nonetheless, both shell-model calculations support a $14_1^+ \rightarrow 12_1^+ \rightarrow 10_1^+$ assignment to the 1133-650-keV cascade based on the predicted energy differences. Although the $10_1^+$ state is underpredicted by 423 keV in the SN100PN calculation, the calculated transition energies of 1024 and 685 keV match well the observed 1133- and 650-keV $\gamma$-ray transitions. The $10_2^+$ state is predicted to be 29 keV above the $12_1^+$ state by the PQM130 interaction, and 203 keV above by the SN100PN calculation. Thus, the observed 476-1240-keV cascade might be interpreted as the $(12_2^+,13_1^+) \rightarrow 11_1^+ \rightarrow 10_1^+$ decay. However, no conclusive assignment can be made, since, foremost, the exact position of the $8_1^+$ state with respect to the $10_1^+$ state remains unclear.

Above the $7_1^-$ isomer, the $(7,8,9)^-$ level at 2829 keV may be interpreted as the $8_1^-$ state. Therefore, the 3155-keV state is most probably of spin $9_1^-$. This assignment is also supported by the PQM130 interaction. Figure 9(a) shows the evolution of the positive-parity ground-state band and of $7_1^-$ and $9_1^-$ states along the $N = 78$ isotones from $Z = 50$ to $Z = 64$. Accordingly, positive-parity yrast states along the Xe chain are shown in Fig. 9(b). The newly assigned states are marked with thicker lines. The $9_1^-$, $12_1^+$, and $14_1^+$ candidates in $^{132}$Xe fit the systematics. Moreover, the systematics suggest the 5665-keV level to be interpreted as the $16_1^+$ state. Nonetheless, transposed $8_1^+$ and $10_1^+$ states could also fit into the isotone systematics.

The level structure of the even-odd isotope $^{133}$Xe is more complex. Both interactions reproduce the low-spin positive-parity states generally well but predict several possibly yrare states in a reversed order with regard to the yrast

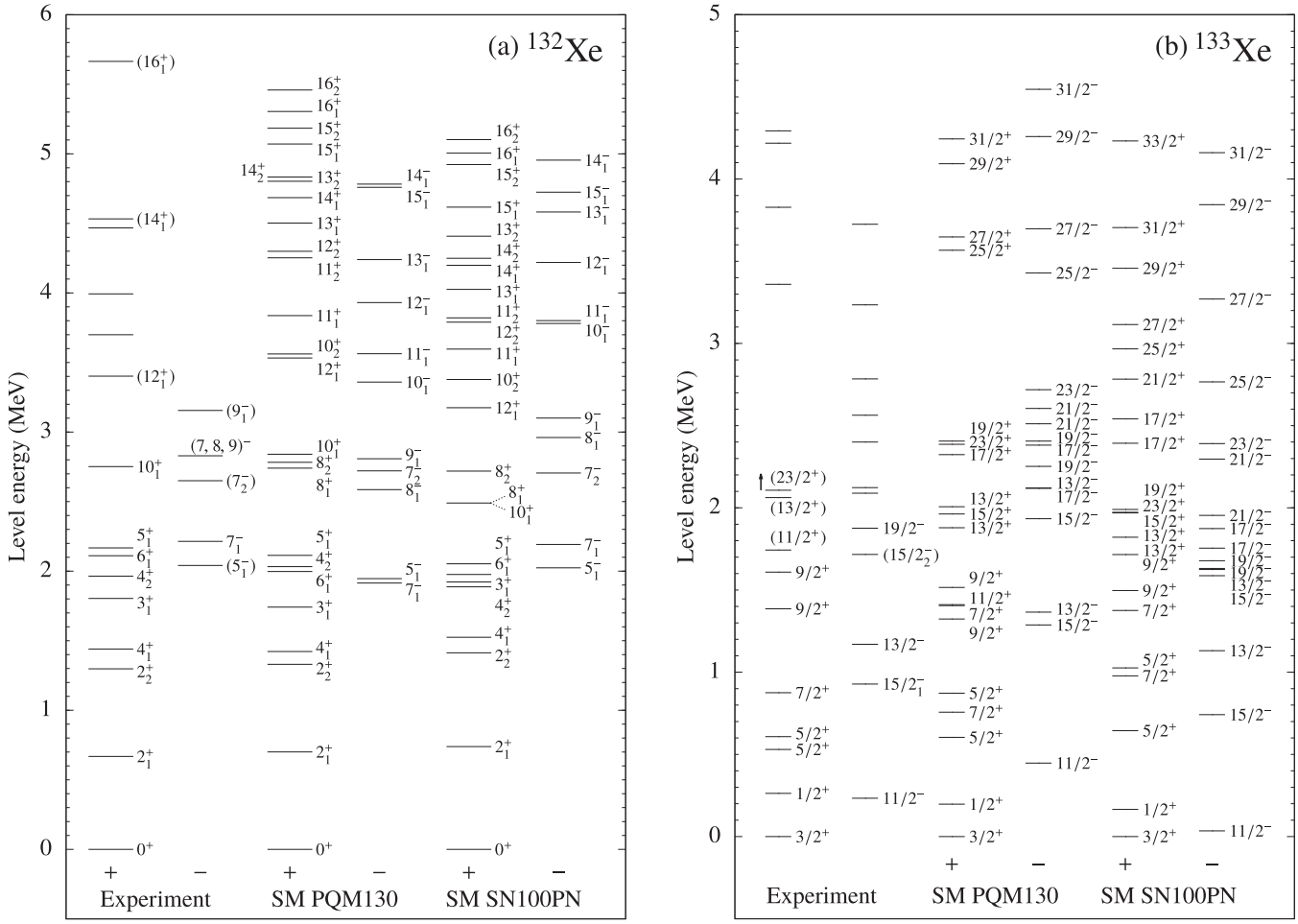


FIG. 8. Comparison of experimental energy spectra with the results of shell-model calculations for (a) $^{132}$Xe and (b) $^{133}$Xe. Experimental energy spectra are shown in the left panels. The middle panels present the results obtained with the PQM130 interaction [4]. The right panels show the computed levels using the SN100PN interaction. For clarity, the states are separated into columns for the negative- and the positive-parity states.

levels. The PQM130 interaction overpredicts the 233-keV $11/2^-_1$ state by 214 keV while the SN100PN interaction places the $11/2^-$ state at an excitation energy of only 35 keV. The SN100PN interaction reproduces the $19/2^-_1 \rightarrow 15/2^-_1 \rightarrow 11/2^-_1$ cascade very well. Deviations amount to only 12 and 65 keV for the 695- and 948-keV transitions, respectively. The $23/2^-_1$ state is predicted to be located 766 or 466 keV above the $19/2^-_1$ state by the SN100PN and the PQM130 interactions, respectively. Additionally, the $21/2^-_1 \rightarrow 19/2^-_1$ transition is computed as $E_\gamma = 329$ keV by the SN100PN or $E_\gamma = 259$ keV by the PQM130 interaction. Therefore, the novel 908-keV $\gamma$-ray transition may be assigned to the decay of the $23/2^-_1$ state. The 465-468-1254-keV cascade, unconnected to any other band, implies the existence of an isomer with a half-life of $T_{1/2} \gg 1$ $\mu$s in $^{133}$Xe. A prompt character excludes the 908-keV transition as following an isomeric decay. Hence, the newly observed isomer is placed at $2107 + x$ keV. Excluding a nonobserved transition, it could decay either via a 440-247-keV cascade or via the 231-keV transition to the $19/2^-_1$ state. An isomeric $J^\pi = 19/2^+_1$ state with a half-life of 14(3) ns, decaying into the $19/2^-$ state, is observed in the neighboring isotope $^{131}$Xe [27]. The $(23/2^+)$ state is observed well above the isomer in this nucleus. Nevertheless, in both $^{133}$Xe and the $-2p$ isotone $^{131}$Te, the SN100PN as well as the PQM130 interaction predict the two unobserved $19/2^+_1$ and $21/2^+_1$ states to be above the $23/2^+_1$ state. Therefore, a $23/2^+_1$ assignment to the $(2107 + x)$-keV isomer is most likely. Based on angular correlations, the 247-keV transition needs to be revised to be the decay of either the $19/2^-_2$ or the $21/2^-_1$ state. The $19/2^+ \rightarrow 19/2^-$ or $21/2^+ \rightarrow 19/2^-$ assignments with multipolarity $E1 + (M2)$ cannot be necessarily excluded in the present angular-correlation measurements, but the spin-trap character of the $23/2^+_1$ state, as computed by both shell-model calculations, obstructs this assignment. This makes a 440-247-keV two-step decay via positive-parity states unlikely. Consequently, the 440-keV transition could be explained as the decay of a higher-lying $21/2^-_{1,2}$ state. The decay of the $(23/2^+)$ isomer may proceed via a $21/2^-$ state (via either 231 or 440-247 keV). This requires the presence of a yet unobserved low-energy $\gamma$-ray transition, which could also be highly converted. In fact, the energy difference between the calculated $21/2^-_1$ and $23/2^+_1$ states amounts to only 125 keV in the PQM130 and 19 keV in the SN100PN interaction. Otherwise, the shell-model calculations would also support the

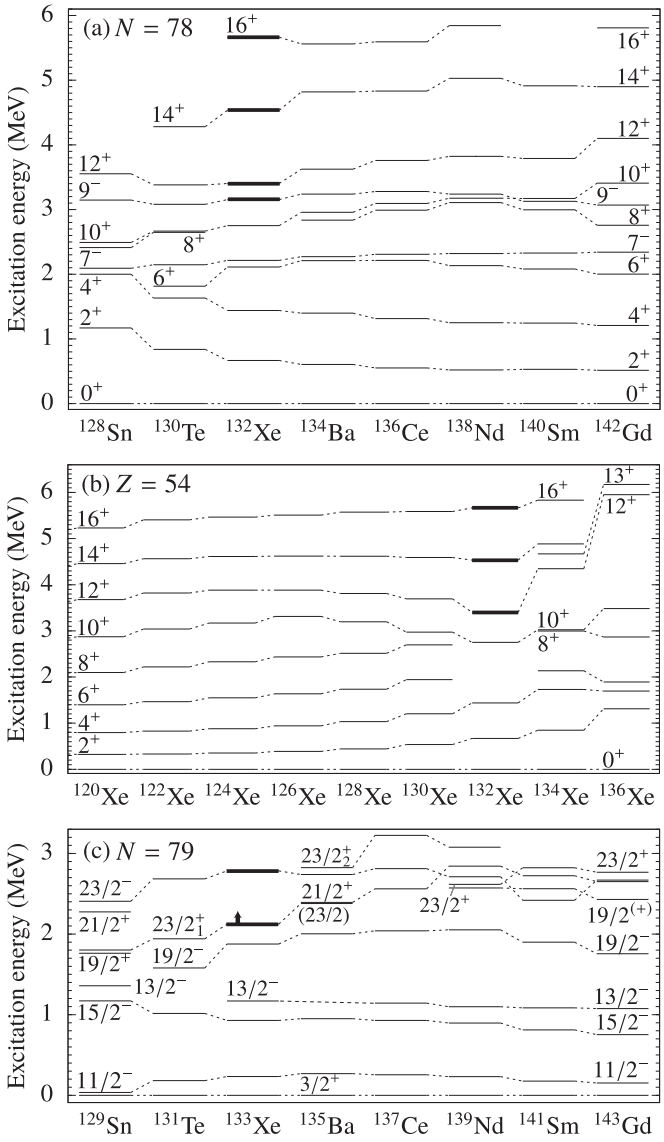


FIG. 9. Evolution of excited states (a) along the $N = 78$ isotones from $Z = 50$ to $Z = 64$, (b) along the Xe isotopes, and (c) along the odd-mass $N = 79$ isotones. Data are from Refs. [40,69–71]. Newly discovered states are marked with thick lines.

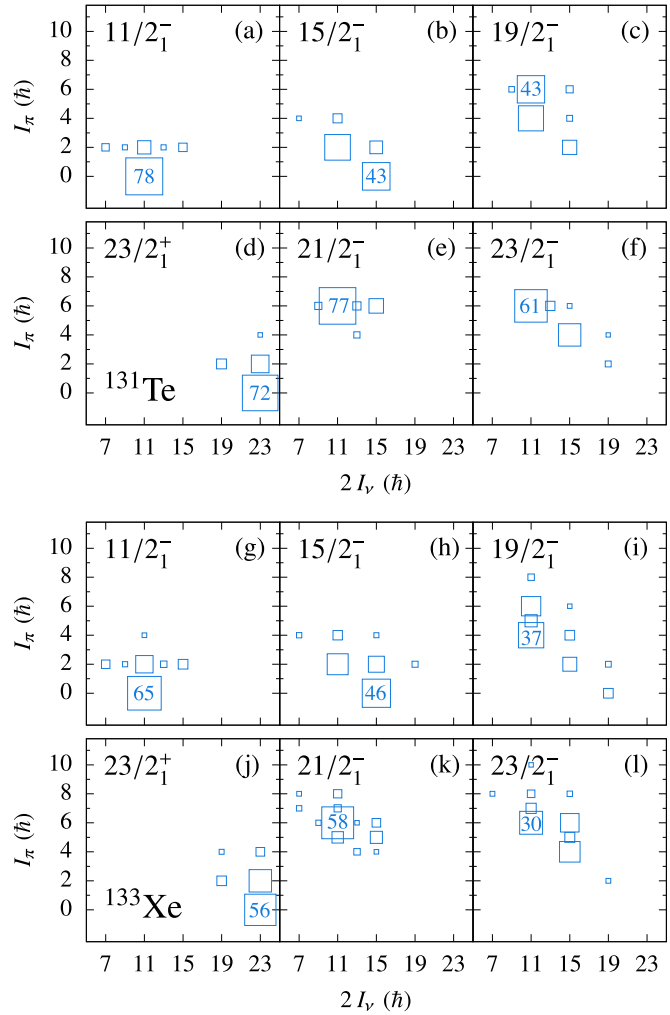


FIG. 10. Decomposition of the total angular momentum $I = I_\pi \otimes I_\nu$ of the SN100PN calculation into its proton and neutron components for several selected negative-parity states as well as the $J^\pi = 23/2^+$ isomer candidate in (a) to (f) $^{131}$Te and (g) to (l) $^{133}$Xe. Strongest components are labeled with corresponding percentages.

231-keV transition to be a long-lived $(23/2^+) \rightarrow 19/2^-_1$ decay with an assumed $M2$ multipolarity. Considering the single-step decay via a 361-keV $\gamma$ ray in $^{131}$Te, isotone systematics suggest the 231-keV transition to follow the $(2107 + x)$-keV isomer decay. In $^{133}$Xe, for $E_\gamma = 231$ keV, the half-lives corresponding to one Weisskopf unit are 1.8 $\mu$s for an $M2$ and 32 ms for an $E3$ transition. Without experimental lifetime information, there is yet no decisive distinction between these possibilities. In the case of a 231-keV transition with pure $M2$ character, the reduced transition strength is constrained to $B(M2; 23/2^+_1 \rightarrow 19/2^-_1) < 1.4$ W.u.

The nuclear structures of $^{133}$Xe and the $-2p$ isotone $^{131}$Te have similar characteristics. Figure 10 shows the decomposition of the total angular momentum $I = I_\pi \otimes I_\nu$ into its proton and neutron components for several selected states in these two nuclei using the SN100PN interaction. Although more fragmented in $^{133}$Xe, the structures of the negative-parity states above $J^\pi = 11/2^-_1$ resemble the ones in $^{131}$Te. The SN100PN interaction predicts the $23/2^+_1$ state in $^{133}$Xe to predominantly have 56% stretched $\nu\, 23/2^+ \otimes \pi\, 0^+$ and 29% $\nu\, 23/2^+ \otimes \pi\, 2^+$ configurations. Neutron $\nu(h^{-2}_{11/2}d^{-1}_{3/2})$ components account for 75% of the configurations. Significant proton configurations coupled to this neutron configuration are 33% of $\pi g^4_{7/2}$, 23% of $\pi(g^3_{7/2}d^1_{5/2})$, and 8% of $\pi(g^2_{7/2}h^2_{11/2})$. Also, the occupation numbers of the PQM130 calculation support a dominant $\nu(h^{-2}_{11/2}d^{-1}_{3/2})$ neutron configuration. In the $^{131}$Te isotone, the SN100PN interaction locates the $23/2^+_1$ state at 1870 keV, close to the experimental value of 1941 keV. Here, the dominant configuration is 69% $\nu(h^{-2}_{11/2}d^{-1}_{3/2}) \otimes \pi g^2_{7/2}$. The stretched $\nu\, 23/2 \otimes \pi\, 0^+$ character in the decomposition of the $23/2^+_1$ state strongly hinders a decay to the other states whose neutron configurations involve an $I_\nu = 11/2$ spin. The SN100PN interaction computes the $B(E2; 19/2^-_1 \rightarrow 15/2^-_1)$ value to be

154 $e^2$fm$^4$ in $^{131}$Te and reproduces the experimental transition strength of $B(E2; 19/2_1^- \rightarrow 15/2_1^-) = 139^{+54}_{-30}$ $e^2$fm$^4$ employing standard effective charges of $e_\pi = 1.5e$ and $e_\nu = 0.5e$. However, the small experimental $B(M2; 23/2^+ \rightarrow 19/2^-)$ value of $1.9 \times 10^{-6}$ W.u. in $^{131}$Te is overpredicted by two orders of magnitude ($8.8 \times 10^{-4}$ W.u.) considering free nuclear $g$ factors. A similar calculation for $^{133}$Xe yields a branching ratio of 81.2% for the $23/2_1^+ \rightarrow 19/2_1^-$ decay. The corresponding theoretical $M2$ transition strength is $3.4 \times 10^{-3}$ W.u. Moreover, the transition strength to the $19/2_2^-$ state, predicted to be 54 keV higher in energy than the calculated $19/2_1^-$ state, is computed to be $1.8 \times 10^{-3}$ W.u.

Similar to the $N = 78$ chain, Fig. 9(c) presents the evolution of several excited states along the $N = 79$ isotones. The novel $23/2_1^+$ candidate fits well into the isotone systematics. As yet, no $19/2^+$ and $21/2^+$ states have been observed in $^{131}$Te, supporting the validity of both shell-model calculations, which locate these levels above the $23/2_1^+$ state. The presence of isomeric $(23/2^+)$ states in the energy regime below 2.5 MeV is discontinued in $^{135}$Ba and $^{137}$Ce, before emerging again in $^{139}$Nd. However, the 2389-keV state in $^{135}$Ba, which was assigned with spin $J = (21/2)$ by both Che *et al.* [72] and Cluff [70], later revised to spin $J = (23/2)$ by Kumar *et al.* [38], could be an isomer candidate. Higher-lying (first excited) $23/2^+$ states are known in $^{135}$Ba and $^{137}$Ce which do not fit the $N = 79$ systematics. Besides, the recent discovery of the 277(2)-ns $J^\pi = 23/2^+$ isomer in $^{139}$Nd [30] results in a smooth onset of $23/2^+$ states along the isotone chain from the high-$Z$ side. Therefore, the existence of a lower-lying first $23/2^+$ state, possibly isomeric, might be anticipated at approximately 2.6 MeV in $^{137}$Ce.

## V. CONCLUSIONS

In summary, the high-spin level schemes of $^{132}$Xe and $^{133}$Xe were extended to excitation energies of 5665 and $4293 + x$ keV, respectively. The observation of a band unconnected to any known $\gamma$-ray cascade corroborates the existence of a long-lived isomer in $^{133}$Xe. Based on isotonic systematics, shell-model calculations, and comparisons of in-beam and stopped-beam experiments, a minimum excitation energy of $E = 2107 + x$ keV is deduced for this state, and a spin-parity assignment of $J^\pi = (23/2^+)$ is suggested. The half-life is estimated to be $T_{1/2} \gg 1$ $\mu$s. This observation of a $(23/2^+)$ isomer fills in a missing cornerstone along the $N = 79$ isotones between $^{129}_{50}$Sn, $^{131}_{52}$Te, and $^{139}_{60}$Nd. Future conversion-electron measurements will identify and resolve the multipole character of the isomer decay in $^{133}$Xe. The well-established structure for the $N = 79$ isotonic chain still lacks some information. Specifically, detailed high-spin studies need to be pursued in forthcoming work, with due attention to the onset of $J^\pi = 23/2^+$ isomerism as a function of proton filling in the $gdsh$ orbitals. Thus far, there are no experimentally observed states which populate the $23/2^+$ isomer in the hard-to-reach nucleus $^{131}$Te. Although studies of $^{135}$Ba and $^{137}$Ce were performed up to highest spins and excitation energies, no isomer candidates below 3 MeV were found yet. The observation of a $(23/2^+)$ isomer in this work and the recent observation of a 277(2)-ns isomer in $^{139}$Nd corroborate the existence of $J^\pi = 23/2^+$ isomers also in the aforementioned two nuclei. Hence, thorough searches for isomers in $^{135}$Ba and $^{137}$Ce should be performed in the future to shed light on the onset of isomerism in this region.

## ACKNOWLEDGMENTS

We would like to cordially thank Dr. G. J. Lane (Australian National University) for valuable discussions. Furthermore, we thank the IKP FN Tandem accelerator team for the professional support during the experiment. The research leading to these results has received funding from the German BMBF under Contract No. 05P12PKFNE TP4, from the European Union Seventh Framework Programme FP7/2007-2013 under Grant Agreement No. 262010 - ENSAR, from the Spanish Ministerio de Ciencia e Innovación under Contract No. FPA2011-29854-C04, from the Spanish Ministerio de Economía y Competitividad under Contract No. FPA2014-57196-C5, from the UK Science and Technology Facilities Council (STFC), and from the US National Science Foundation (NSF). E.T. and N.Y. were supported by a Grant-in-Aid for Japan Society for the Promotion of Science (JSPS) Fellows (Grant No. 26.10429). A.V. and L.K. thank the Bonn-Cologne Graduate School of Physics and Astronomy (BCGS) for financial support. One of the authors (A. Gadea) has been supported by the Generalitat Valenciana, Spain, under the grant PROMETEOII/2014/019 and by the EU under the FEDER program.

[1] H. Morinaga and N. L. Lark, Collective excited states in even xenon isotopes, Nucl. Phys. **67**, 315 (1965).
[2] B. A. Brown, N. J. Stone, J. R. Stone, I. S. Towner, and M. Hjorth-Jensen, Magnetic moments of the $2_1^+$ states around $^{132}$Sn, Phys. Rev. C **71**, 044317 (2005).
[3] K. Higashiyama and N. Yoshinaga, Pair-truncated shell-model analysis of nuclei around mass 130, Phys. Rev. C **83**, 034321 (2011).
[4] E. Teruya, N. Yoshinaga, K. Higashiyama, and A. Odahara, Shell-model calculations of nuclei around mass 130, Phys. Rev. C **92**, 034320 (2015).
[5] L. Coraggio, A. Covello, A. Gargano, N. Itaco, and T. T. S. Kuo, Shell-model study of the $N = 82$ isotonic chain with a realistic effective Hamiltonian, Phys. Rev. C **80**, 044320 (2009).
[6] E. Caurier, F. Nowacki, A. Poves, and K. Sieja, Collectivity in the light xenon isotopes: A shell model study, Phys. Rev. C **82**, 064304 (2010).
[7] Y. Utsuno, T. Otsuka, N. Shimizu, M. Honma, T. Mizusaki, Y. Tsunoda, and T. Abe, Recent shell-model results for exotic nuclei, EPJ Web Conf. **66**, 02106 (2014).
[8] Y. Khazov, A. A. Rodionov, S. Sakharov, and B. Singh, Nuclear data sheets for $A = 132$, Nucl. Data Sheets **104**, 497 (2005).

[9] Y. Khazov, A. Rodionov, and F. G. Kondev, Nuclear data sheets for $A = 133$, Nucl. Data Sheets **112**, 855 (2011).

[10] L. Coquard, N. Pietralla, G. Rainovski, T. Ahn, L. Bettermann, M. P. Carpenter, R. V. F. Janssens, J. Leske, C. J. Lister, O. Möller, W. Rother, V. Werner, and S. Zhu, Evolution of the mixed-symmetry $2^+_{1,\mathrm{ms}}$ quadrupole-phonon excitation from spherical to $\gamma$-soft Xe nuclei, Phys. Rev. C **82**, 024317 (2010).

[11] E. E. Peters, T. J. Ross, S. F. Ashley, A. Chakraborty, B. P. Crider, M. D. Hennek, S. H. Liu, M. T. McEllistrem, S. Mukhopadhyay, F. M. Prados-Estévez, A. P. D. Ramirez, J. S. Thrasher, and S. W. Yates, $0^+$ states in $^{130,132}$Xe: A search for E(5) behavior, Phys. Rev. C **94**, 024313 (2016).

[12] A. Kerek, A. Luukko, M. Grecescu, and J. Sztarkier, Two- and three-quasiparticle states in $^{132}$Xe and $^{131}$Xe, Nucl. Phys. A **172**, 603 (1971).

[13] T. Lönnroth and J. Kumpulainen and C. Tuokko, One- and three-quasiparticle states in $^{127,129,131,133}$Xe and their coexistence with band structures, Phys. Scr. **27**, 228 (1983).

[14] R. Broda, Spectroscopic studies with the use of deep-inelastic heavy-ion reactions, J. Phys. G **32**, R151 (2006).

[15] A. Vogt, B. Birkenbach, P. Reiter, L. Corradi, T. Mijatović, D. Montanari, S. Szilner, D. Bazzacco, M. Bowry, A. Bracco, B. Bruyneel, F. C. L. Crespi, G. de Angelis, P. Désesquelles, J. Eberth, E. Farnea, E. Fioretto, A. Gadea, K. Geibel, A. Gengelbach, A. Giaz, A. Görgen, A. Gottardo, J. Grebosz, H. Hess, P. R. John, J. Jolie, D. S. Judson, A. Jungclaus, W. Korten, S. Leoni, S. Lunardi, R. Menegazzo, D. Mengoni, C. Michelagnoli, G. Montagnoli, D. Napoli, L. Pellegri, G. Pollarolo, A. Pullia, B. Quintana, F. Radeck, F. Recchia, D. Rosso, E. Şahin, M. D. Salsac, F. Scarlassara, P.-A. Söderström, A. M. Stefanini, T. Steinbach, O. Stezowski, B. Szpak, Ch. Theisen, C. Ur, J. J. Valiente-Dobón, V. Vandone, and A. Wiens, Light and heavy transfer products in $^{136}$Xe + $^{238}$U multinucleon transfer reactions, Phys. Rev. C **92**, 024619 (2015).

[16] L. Atanasova, D. L. Balabanski, S. K. Chamoli, M. Hass, G. S. Simpson, D. Bazzacco, F. Becker, P. Bednarczyk, G. Benzoni, N. Blasi, A. Blazhev, A. Bracco, C. Brandau, L. Caceres, F. Camera, F. C. L. Crespi, P. Detistov, P. Doornenbal, C. Fahlander, E. Farnea, G. Georgiev, J. Gerl, K. A. Gladnishki, M. Górska, J. Grebosz, R. Hoischen, G. Ilie, M. Ionescu-Bujor, A. Iordachescu, A. Jungclaus, G. Lo Bianco, M. Kmiecik, I. Kojouharov, N. Kurz, S. Lakshmi, R. Lozeva, A. Maj, D. Montanari, G. Neyens, M. Pfützner, S. Pietri, Zs. Podolyák, W. Prokopowicz, D. Rudolph, G. Rusev, T. R. Saito, A. Saltarelli, H. Schaffner, R. Schwengner, S. Tashenov, J. J. Valiente-Dobón, N. Vermeulen, J. Walker, E. Werner-Malento, O. Wieland, H. J. Wollersheim, H. Grawe, and M. Hjorth-Jensen, $g$-factor measurements at RISING: The cases of $^{127}$Sn and $^{128}$Sn, Europhys. Lett. **91**, 42001 (2010).

[17] J. Genevey, J. A. Pinston, C. Foin, M. Rejmund, R. F. Casten, H. Faust, and S. Oberstedt, Conversion electron measurements of isomeric transitions in $^{130,132}$Te and $^{134}$Xe, Phys. Rev. C **63**, 054315 (2001).

[18] M. v. Hartrott, J. Hadijuana, K. Nishiyama, D. Quitmann, D. Riegel, and H. Schweickert, Nuclear spin relaxation of Xe in liquid Te, Z. Phys. A **278**, 303 (1976).

[19] T. Morek, H. Beuscher, B. Bochev, D. R. Haenni, R. M. Lieder, T. Kutsarova, M. Müller-Veggian, and A. Neskakis, Isomeric states in $^{134}$Ba, Z. Phys. A **298**, 267 (1980).

[20] M. Müller-Veggian, H. Beuscher, R. M. Lieder, Y. Gono, D. R. Haenni, A. Neskakis, and C. Mayer-Böricke, $10^+$ isomers observed in even-even 78-neutron nuclei, Z. Phys. A **290**, 43 (1979).

[21] W. Starzecki, G. De Angelis, B. Rubio, J. Styczen, K. Zuber, H. Güven, W. Urban, W. Gast, P. Kleinheinz, S. Lunardi, F. Soramel, A. Facco, C. Signorini, M. Morando, W. Meczynski, A. M. Stefanini, and G. Fortuna, Prolate and oblate $10^+$ isomers in $^{140}$Sm$_{78}$ and $^{142}$Gd$_{78}$, Phys. Lett. B **200**, 419 (1988).

[22] M. G. Procter, D. M. Cullen, C. Scholey, B. Niclasen, P. J. R. Mason, S. V. Rigby, J. A. Dare, A. Dewald, P. T. Greenlees, H. Iwasaki, U. Jakobsson, P. M. Jones, R. Julin, S. Juutinen, S. Ketelhut, M. Leino, N. M. Lumley, O. Möller, M. Nyman, P. Peura, T. Pissulla, A. Puurunen, P. Rahkila, W. Rother, P. Ruotsalainen, J. Sarén, J. Sorri, and J. Uusitalo, Lifetime measurements and shape coexistence in $^{144}$Dy, Phys. Rev. C **81**, 054320 (2010).

[23] H. F. Brinckmann, C. Heiser, and W. D. Fromm, Ein hochangeregter isomerer Kernzustand in $^{132}$Xe, Nucl. Phys. A **96**, 318 (1967).

[24] J. J. Valiente-Dobón, P. H. Regan, C. Wheldon, C. Y. Wu, N. Yoshinaga, K. Higashiyama, J. F. Smith, D. Cline, R. S. Chakrawarthy, R. Chapman, M. Cromaz, P. Fallon, S. J. Freeman, A. Görgen, W. Gelletly, A. Hayes, H. Hua, S. D. Langdown, I. Y. Lee, X. Liang, A. O. Macchiavelli, C. J. Pearson, Zs. Podolyák, G. Sletten, R. Teng, D. Ward, D. D. Warner, and A. D. Yamamoto, $^{136}$Ba studied via deep-inelastic collisions: Identification of the $(\nu h_{11/2})^{-2}_{10+}$ isomer, Phys. Rev. C **69**, 024316 (2004).

[25] J. Timar, Z. Elekes, and B. Singh, Nuclear data sheets for $A = 129$, Nucl. Data Sheets **121**, 143 (2014).

[26] J. Genevey, J. A. Pinston, C. Foin, M. Rejmund, H. Faust, and B. Weiss, High spin isomers in $^{129}$Sn and $^{130}$Sb, Phys. Rev. C **65**, 034322 (2002).

[27] Y. Khazov, I. Mitropolsky, and A. Rodionov, Nuclear data sheets for $A = 131$, Nucl. Data Sheets **107**, 2715 (2006).

[28] P. K. Joshi, B. Singh, S. Singh, and A. K. Jain, Nuclear data sheets for $A = 139$, Nucl. Data Sheets **138**, 1 (2016).

[29] A. Astier, M. G. Porquet, Ts. Venkova, Ch. Theisen, G. Duchêne, F. Azaiez, G. Barreau, D. Curien, I. Deloncle, O. Dorvaux, B. J. P. Gall, M. Houry, R. Lucas, N. Redon, M. Rousseau, and O. Stézowski, High-spin structures of $^{124-131}$Te: Competition of proton- and neutron-pair breakings, Eur. Phys. J. **50**, 1 (2014).

[30] A. Vancraeyenest, C. M. Petrache, D. Guinet, P. T. Greenlees, U. Jakobsson, R. Julin, S. Juutinen, S. Ketelhut, M. Leino, M. Nyman, P. Peura, P. Rahkila, P. Ruotsalainen, J. Saren, C. Scholey, J. Sorri, J. Uusitalo, P. Jones, C. Ducoin, P. Lautesse, C. Mancuso, N. Redon, O. Stezowski, P. Désesquelles, R. Leguillon, A. Korichi, T. Zerrouki, D. Curien, and A. Takashima, Identification of new transitions feeding the high-spin isomers in $^{139}$Nd and $^{140}$Nd nuclei, Phys. Rev. C **87**, 064303 (2013).

[31] J. A. Pinston, C. Foin, J. Genevey, R. Béraud, E. Chabanat, H. Faust, S. Oberstedt, and B. Weiss, Microsecond isomers in $^{125,127,129}$Sn, Phys. Rev. C **61**, 024312 (2000).

[32] R. L. Lozeva, G. S. Simpson, H. Grawe, G. Neyens, L. A. Atanasova, D. L. Balabanski, D. Bazzacco, F. Becker, P. Bednarczyk, G. Benzoni, N. Blasi, A. Blazhev, A. Bracco, C. Brandau, L. Cáceres, F. Camera, S. K. Chamoli, F. C. L. Crespi, J.-M. Daugas, P. Detistov, M. De Rydt, P. Doornenbal, C. Fahlander, E. Farnea, G. Georgiev, J. Gerl, K. A. Gladnishki, M. Górska, J. Grębosz, M. Hass, R. Hoischen, G. Ilie, M. Ionescu-Bujor, A. Iordachescu, J. Jolie, A. Jungclaus, M. Kmiecik, I. Kojouharov, N. Kurz, S. P. Lakshmi, G. Lo Bianco, S. Mallion,

A. Maj, D. Montanari, O. Perru, M. Pfützner, S. Pietri, J. A. Pinston, Zs. Podolyák, W. Prokopowicz, D. Rudolph, G. Rusev, T. R. Saitoh, A. Saltarelli, H. Schaffner, R. Schwengner, S. Tashenov, K. Turzó, J. J. Valiente-Dobón, N. Vermeulen, J. Walker, E. Werner-Malento, O. Wieland, and H.-J. Wollersheim, New sub-$\mu$s isomers in $^{125,127,129}$Sn and isomer systematics of $^{124-130}$Sn, Phys. Rev. C **77**, 064313 (2008).

[33] C. T. Zhang, P. Bhattacharyya, P. J. Daly, Z. W. Grabowski, R. H. Mayer, M. Sferrazza, R. Broda, B. Fornal, W. Królas, T. Pawlat, D. Bazzacco, S. Lunardi, C. Rossi Alvarez, and G. de Angelis, Yrast excitations in $A = 126$–131 Te nuclei from deep inelastic $^{130}$Te + $^{64}$Ni reactions, Nucl. Phys. A **628**, 386 (1998).

[34] B. Fogelberg, H. Mach, H. Gausemel, J. P. Omtvedt, and K. A. Mezilev, New high spin isomers obtained in thermal fission, in *The Second International Workshop on Nuclear Fission and Fission-Product Spectroscopy, April 1998, Seyssins, France*, edited by G. Fioni, H. Faust, S. Oberstedt, and F.-J. Hambsch, AIP Conf. Proc. No. 447 (AIP, New York, 1998), p. 191.

[35] M. Müller-Veggian, H. Beuscher, D. R. Haenni, R. M. Lieder, A. Neskakis, and C. Mayer-Böricke, Investigation of high-spin states in $^{138,139}$Nd, Nucl. Phys. A **344**, 89 (1980).

[36] M. Ferraton, R. Bourgain, C. M. Petrache, D. Verney, F. Ibrahim, N. de Séréville, S. Franchoo, M. Lebois, C. Phan Viet, L. Sagui, I. Stefan, J. F. Clavelin, and M. Vilmay, Lifetime measurement of the six-quasiparticle isomer in $^{140}$Nd and evidence for an isomer above the $19/2^+$ state in $^{139}$Nd, Eur. Phys. J. A **35**, 167 (2008).

[37] M. Müller-Veggian, Y. Gono, R. M. Lieder, A. Neskakis, and C. Mayer-Böricke, High-spin states and isomers in $^{136,137,138}$Ce, Nucl. Phys. A **304**, 1 (1978).

[38] S. Kumar, A. K. Jain, Alpana Goel, S. S. Malik, R. Palit, H. C. Jain, I. Mazumdar, P. K. Joshi, Z. Naik, A. Dhal, T. Trivedi, I. Mehrotra, S. Appannababu, L. Chaturvedi, V. Kumar, R. Kumar, D. Negi, R. P. Singh, S. Muralithar, R. K. Bhowmik, and S. C. Pancholi, Band structure and shape coexistence in $^{135}_{56}$Ba$_{79}$, Phys. Rev. C **81**, 067304 (2010).

[39] T. Bhattacharjee, S. Chanda, A. Mukherjee, S. Bhattacharyya, S. K. Basu, S. S. Ghugre, U. D. Pramanik, R. P. Singh, S. Muralithar, N. Madhavan, J. J. Das, and R. K. Bhowmik, Multi-quasiparticle bands in $^{137}$Ce, Phys. Rev. C **78**, 024304 (2008).

[40] Evaluated Nuclear Structure Data File (ENSDF), http://www.nndc.bnl.gov/ensdf/

[41] S. Akkoyun *et al.*, AGATA – Advanced GAmma Tracking Array, Nucl. Instrum. Methods Phys. Res. A **668**, 26 (2012).

[42] A. M. Stefanini, L. Corradi, G. Maron, A. Pisent, M. Trotta, A. M. Vinodkumar, S. Beghini, G. Montagnoli, F. Scarlassara, G. F. Segato, A. De Rosa, G. Inglima, D. Pierroutsakou, M. Romoli, M. Sandoli, G. Pollarolo, and A. Latina, The heavy-ion magnetic spectrometer PRISMA, Nucl. Phys. A **701**, 217 (2002).

[43] S. Szilner, C. A. Ur, L. Corradi, N. Marginean, G. Pollarolo, A. M. Stefanini, S. Beghini, B. R. Behera, E. Fioretto, A. Gadea, B. Guiot, A. Latina, P. Mason, G. Montagnoli, F. Scarlassara, M. Trotta, G. de Angelis, F. Della Vedova, E. Farnea, F. Haas, S. Lenzi, S. Lunardi, R. Marginean, R. Menegazzo, D. R. Napoli, M. Nespolo, I. V. Pokrovsky, F. Recchia, M. Romoli, M.-D. Salsac, N. Soić, and J. J. Valiente-Dobón, Multinucleon transfer reactions in closed-shell nuclei, Phys. Rev. C **76**, 024604 (2007).

[44] L. Corradi, S. Szilner, G. Pollarolo, D. Montanari, E. Fioretto, A. M. Stefanini, J. J. Valiente-Dobón, E. Farnea, C. Michelagnoli, G. Montagnoli, F. Scarlassara, C. A. Ur, T. Mijatović, D. Jelavić Malenica, N. Soić, and F. Haas, Multinucleon transfer reactions: Present status and perspectives, Nucl. Instrum. Methods Phys. Res. B **317, Part B**, 743 (2013).

[45] I.-Y. Lee, The GAMMASPHERE, Nucl. Phys. A **520**, c641 (1990).

[46] M. W. Simon, D. Cline, C. Y. Wu, R. W. Gray, R. Teng, and C. Long, CHICO, a heavy ion detector for Gammasphere, Nucl. Instrum. Methods Phys. Res. A **452**, 205 (2000).

[47] L. Netterdon, V. Derya, J. Endres, C. Fransen, A. Hennig, J. Mayer, C. Müller-Gatermann, A. Sauerwein, P. Scholz, M. Spieker, and A. Zilges, The $\gamma$-ray spectrometer HORUS and its applications for nuclear astrophysics, Nucl. Instrum. Methods Phys. Res. A **754**, 94 (2014).

[48] M. W. Reed, G. J. Lane, G. D. Dracoulis, F. G. Kondev, A. E. Stuchbery, A. P. Byrne, M. P. Carpenter, P. Chowdhury, S. S. Hota, R. O. Hughes, R. V. F. Janssens, T. Lauritsen, C. J. Lister, D. Seweryniak, E. C. Simpson, H. Watanabe, and S. Zhu, High-spin and delayed structure of $^{133}$Xe (unpublished).

[49] A. Gadea, E. Farnea, J. J. Valiente-Dobón, B. Million, D. Mengoni, D. Bazzacco, F. Recchia, A. Dewald, Th. Pissulla, W. Rother, G. de Angelis *et al.*, Conceptual design and infrastructure for the installation of the first AGATA sub-array at LNL, Nucl. Instrum. Methods Phys. Res. A **654**, 88 (2011).

[50] A. Wiens, H. Hess, B. Birkenbach, B. Bruyneel, J. Eberth, D. Lersch, G. Pascovici, P. Reiter, and H.-G. Thomas, The AGATA triple cluster detector, Nucl. Instrum. Methods Phys. Res. A **618**, 223 (2010).

[51] B. Bruyneel, B. Birkenbach, and P. Reiter, Pulse shape analysis and position determination in segmented HPGe detectors: The AGATA detector library, Eur. Phys. J. A **52**, 70 (2016).

[52] A. Lopez-Martens, K. Hauschild, A. Korichi, J. Roccaz, and J.-P. Thibaud, $\gamma$-ray tracking algorithms: A comparison, Nucl. Instrum. Methods Phys. Res. A **533**, 454 (2004).

[53] A. B. Brown, C. W. Snyder, W. A. Fowler, and C. C. Lauritsen, Excited States of the Mirror Nuclei, $^7$Li and $^7$Be, Phys. Rev. **82**, 159 (1951).

[54] D. C. Radford, ESCL8R and LEVIT8R: Software for interactive graphical analysis of HPGe coincidence data sets, Nucl. Instrum. Methods Phys. Res. A **361**, 297 (1995).

[55] N. Saed-Samii, Lifetime measurements using the FATIMA array in combination with EXOGAM@ILL, Diplomarbeit, Universität zu Köln, 2013 (unpublished).

[56] N. Saed-Samii, computer code SOCO-V2, 2017, https://gitlab.ikp.uni-koeln.de/nima/soco-v2.

[57] J. Theuerkauf, Die Analyse von zwei- und mehrdimensionalen $\gamma\gamma$-Koinzidenzspektren an Beispielen aus Hochspinexperimenten in der Massengegend um $^{146}$Gd, Ph.D. thesis, Universität zu Köln, 1994.

[58] A. Linnemann, Das HORUS-Würfelspektrometer und Multiphononanregungen in $^{106}$Cd, Ph.D. thesis, Universität zu Köln, 2006.

[59] I. Wiedenhöver, computer code CORLEONE, 1997.

[60] I. Wiedenhöver, O. Vogel, H. Klein, A. Dewald, P. von Brentano, J. Gableske, R. Krücken, N. Nicolay, A. Gelberg, P. Petkov, A. Gizon, J. Gizon, D. Bazzaco, C. Rossi Alvarez, G. de Angelis, S. Lunardi, P. Pavan, D. R. Napoli, S. Frauendorf, F. Dönau, R. V. F. Janssens, and M. P. Carpenter, Detailed angular correlation analysis with $4\pi$ spectrometers: Spin determinations and multipolarity mixing measurements in $^{128}$Ba, Phys. Rev. C **58**, 721 (1998).

[61] K. S. Krane and R. M. Steffen, Determination of the $E2/M1$ multipole mixing ratios of the gamma transitions in $^{110}$Cd, Phys. Rev. C **2**, 724 (1970).

[62] K. S. Krane, R. M. Steffen, and R. M. Wheeler, Directional correlations of gamma radiations emitted from nuclear states oriented by nuclear reactions or cryogenic methods, At. Data Nucl. Data Tables **11**, 351 (1973).

[63] L. Bettermann, C. Fransen, S. Heinze, J. Jolie, A. Linnemann, D. Mücher, W. Rother, T. Ahn, A. Costin, N. Pietralla, and Y. Luo, Candidates for the one-phonon mixed-symmetry state in $^{130}$Xe, Phys. Rev. C **79**, 034315 (2009).

[64] M. Dikšić, L. Yaffe, and D. G. Sarantites, Identification and decay characteristics of $^{132}$I$^{m}$, Phys. Rev. C **10**, 1172 (1974).

[65] B. A. Brown and W. D. M. Rae, The shell-model code NuShellX@MSU, Nucl. Data Sheets **120**, 115 (2014).

[66] R. Machleidt, F. Sammarruca, and Y. Song, Nonlocal nature of the nuclear force and its impact on nuclear structure, Phys. Rev. C **53**, R1483 (1996).

[67] K. Higashiyama, N. Yoshinaga, and K. Tanabe, Shell model study of backbending phenomena in Xe isotopes, Phys. Rev. C **65**, 054317 (2002).

[68] H. Kusakari, K. Kitao, K. Sato, M. Sugawara, and H. Katsuragawa, High-spin states in even-mass Xe nuclei and backbending phenomena, Nucl. Phys. A **401**, 445 (1983).

[69] A. Vogt, B. Birkenbach, P. Reiter, A. Blazhev, M. Siciliano, J. J. Valiente-Dobón, C. Wheldon, D. Bazzacco, M. Bowry, A. Bracco, B. Bruyneel, R. S. Chakrawarthy, R. Chapman, D. Cline, L. Corradi, F. C. L. Crespi, M. Cromaz, G. de Angelis, J. Eberth, P. Fallon, E. Farnea, E. Fioretto, S. J. Freeman, A. Gadea, K. Geibel, W. Gelletly, A. Gengelbach, A. Giaz, A. Görgen, A. Gottardo, A. B. Hayes, H. Hess, H. Hua, P. R. John, J. Jolie, A. Jungclaus, W. Korten, I. Y. Lee, S. Leoni, X. Liang, S. Lunardi, A. O. Macchiavelli, R. Menegazzo, D. Mengoni, C. Michelagnoli, T. Mijatović, G. Montagnoli, D. Montanari, D. Napoli, C. J. Pearson, L. Pellegri, Zs. Podolyák, G. Pollarolo, A. Pullia, F. Radeck, F. Recchia, P. H. Regan, E. Şahin, F. Scarlassara, G. Sletten, J. F. Smith, P.-A. Söderström, A. M. Stefanini, T. Steinbach, O. Stezowski, S. Szilner, B. Szpak, R. Teng, C. Ur, V. Vandone, D. Ward, D. D. Warner, A. Wiens, and C. Y. Wu, High-spin structure of $^{134}$Xe, Phys. Rev. C **93**, 054325 (2016).

[70] W. T. Cluff, The High-Spin Structure of $^{134,135}$Ba and $^{120}$Te, Ph.D. thesis, Florida State University, 2008.

[71] A. Astier, M.-G. Porquet, Ts. Venkova, D. Verney, Ch. Theisen, G. Duchêne, F. Azaiez, G. Barreau, D. Curien, I. Deloncle, O. Dorvaux, B. J. P. Gall, M. Houry, R. Lucas, N. Redon, M. Rousseau, and O. Stézowski, High-spin structures of five $N = 82$ isotopes: $^{136}$Xe, $^{137}$Cs, $^{138}$Ba, $^{139}$La, and $^{140}$Ce, Phys. Rev. C **85**, 064316 (2012).

[72] X. L. Che, S. J. Zhu, M. L. Li, Y. J. Chen, Y. N. U, H. B. Ding, L. H. Zhu, X. G. Wu, G. S. Li, C. Y. He, and Y. Liu, High-spin levels based on the $11/2^{-}$ isomer in $^{135}$Ba, Eur. Phys. J. A **30**, 347 (2006).